# Investigation of Scattering Mechanism in Nano-Scale Double Gate $In_{0.53}Ga_{0.47}As$ nMOSFETs by a Deterministic BTE Solver

Shaoyan Di[1], Zhiyuan Lun [1], Pengying Chang[1], Lei Shen[1], Kai Zhao[1,3,*], Tiao Lu[2], Gang Du[1], Xiaoyan Liu[1]
1. Institute of Microelectronics, Peking University, 100871 Beijing, China
2. CAPT, HEDPS, IFSA Collaborative Innovation Center of MoE, LMAM & School of Mathematical Sciences, Peking University, Beijing, China.
3. School of Information and Communication, Beijing Information Science and Technology University, Beijing 100101, China
*Corresponding Author's Email: k.zhao.chn@gmail.com

***Abstract*—we investigate the scattering mechanism in ultra-short double gate $In_{0.53}Ga_{0.47}As$ nMOSFETs by deterministically solving Boltzmann transport equation (BTE). The intra-valley acoustic phonon scattering, optical phonon scattering, inter-valley optical scattering, polar optical scattering, and surface roughness (SR) scattering are considered. The impacts of scattering on the performance of device under high/low biases are compared. Results show that the ballistic ratio ($I_{scat}/I_{ball}$) decreases from 96.8% to 94.5% when the drain bias increases from 0.05V to 0.6V, which is mainly caused by the inter-valley scatterings.**

***Keywords—Boltzmann transport equation (BTE); InGaAs; double gate; scattering;***

## I. Introduction

III-V material is gradually becoming a candidate for the next generation to substitute Si devices [1] because of its small effective mass and consequently, much higher mobility [2, 3]. However, continuing scaling down, the channel length is only several times the mean free path. The electrons can only encounter a few times of scattering. On the other hand, increasing longitudinal electric field will bring in a variety of inter-valley scattering mechanisms because the higher valley can be populated by electrons with enough energy. These factors make it difficult to predict the drive current by the conventional low field mobility or the traditional ballistic approach [4]. In such a circumstance, the scattering properties of modern devices under high electric field have to be reassessed [5]. The BTE can describe carrier transport accurately. Consequently, it is suitable to have an insight into the scattering properties [6]. In this work, a deterministic multi-subband BTE solver [7- 9] is used to evaluate the impact of scattering on the performance of III-V device under various drain biases.

## II. Simulation Method and Device Structure

The deterministic time-dependent BTE solver is based on the positive and flux conservative (PFC) method [10]. The time splitting and dimensional splitting techniques [11] are employed during the iterations of coupled equations. In the solver, the Schrödinger-Poisson iteration is coupled with the BTE to consider the quantum confinement where a 2D Poisson equation and a group of 1D Schrödinger equations are solved self-consistently.

978-1-5090-0818-6/16/$31.00 ©2016 IEEE

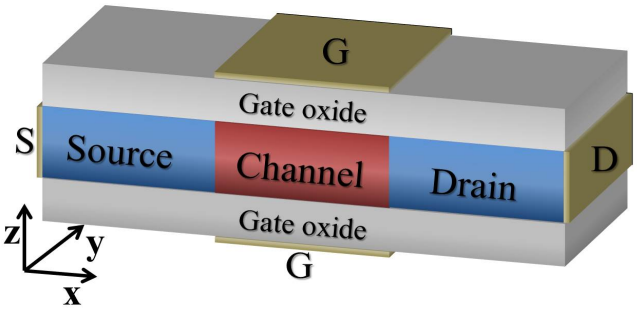


Fig. 1. The device structure. The gate length is 10nm and the film thickness is 5nm. The length of the source and drain is the same as the channel. The EOT is 1nm.

TABLE I
Band and scattering parameters

| Para. | Values | Para. | Values |
|---|---|---|---|
| $m_\Gamma$ | $0.048m_0$ | $D_o$ | $2.053\times10^8$eV/cm |
| $m_{Lt}$ | $0.126m_0$ | $\hbar\omega_0/2\pi$ | 32.88meV |
| $m_{Ll}$ | $1.55m_0$ | $D_{\Gamma,L}$ | $5.41\times10^8$eV/cm |
| $\Delta E_{\Gamma,L}$ | 0.678eV | $\hbar\omega_{\Gamma,L}/2\pi$ | 20.22meV |
| $E_{ac}$ | 5.376eV | $D_{L,L}$ | $6.13\times10^8$eV/cm |
| $\rho$ | $5.51g/cm^3$ | $\hbar\omega_{L,L}/2\pi$ | 22.27meV |
| $v_s$ | $4.73\times10^5$cm/s | $\varepsilon_0$ | 13.96 |
| $\Delta_{SR}$ | 0.5nm | $\varepsilon_{indf}$ | 11.77 |
| $L_{SR}$ | 2nm | | |

The intra-valley acoustic phonon scattering, optical phonon scattering, inter-valley optical scattering [12], polar optical scattering [13], and surface roughness scattering [14] are involved. The band and scattering parameters of $In_{0.53}Ga_{0.47}As$ material are extracted from [15] and listed in Table I. The polar coordination is used in **k** space and the space is separated by 6 uniform angular grids and 150 non-uniform (uniform in magnitude of **k**) grids. The maximum energy is $150k_BT$. The lowest subband in Γ valley and 2 lowest subbands in 4

TABLE II
Structure parameters

| Parameters | Values |
|---|---|
| Channel length | 10nm |
| S/D length | 10nm |
| EOT | 1nm |
| Film thickness | 5nm |
| Channel doping | $10^{17}$cm$^{-3}$ |
| S/D doping | $5\times10^{19}$cm$^{-3}$ |
| dx | 0.2nm |
| dz | 0.1nm |

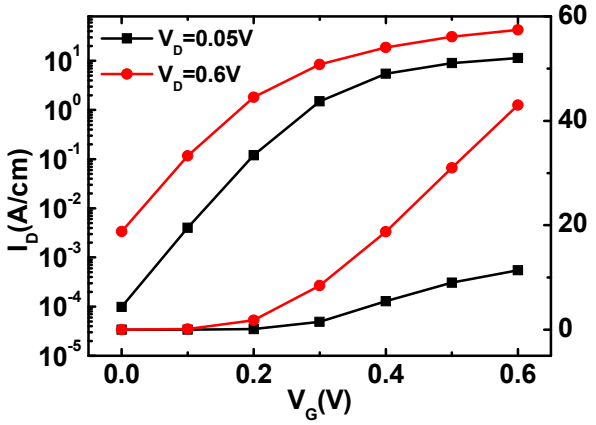


Fig. 2. The $I_D$-$V_G$ curves of the device with the drain voltage of 0.05V and 0.6V, respectively. The off current is set to be $10^{-4}$ A/cm with drain voltage of 0.05V.

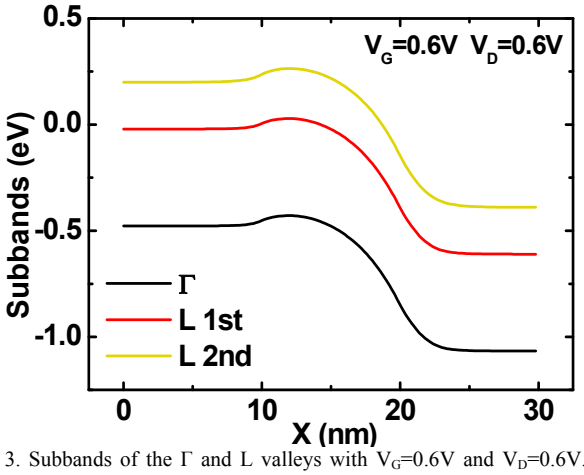


Fig. 3. Subbands of the Γ and L valleys with $V_G$=0.6V and $V_D$=0.6V. The energy gap between the Γ and L valley is smaller than the bulk material because of quantum confinement effect.

equivalent L valleys are considered in the simulation. The Pauli's exclusion principle is also involved.

A 10-nm $In_{0.53}Ga_{0.47}As$ double gate nMOSFET (shown in Fig. 1) is simulated to investigate the impact of scattering. The structure parameters are listed in Table II.

## III. Results and Disscusions

The drain current versus gate voltage under drain biases of 0.05V and 0.6V is shown in Fig.2. The supply voltage is 0.6V according to the ITRS [16]. The off current is set to be $10^{-4}$ A/cm with the drain voltage of 0.05V by shifting the work function. The SS is 73.3mV/dec and the DIBL is 163.6mV/V.

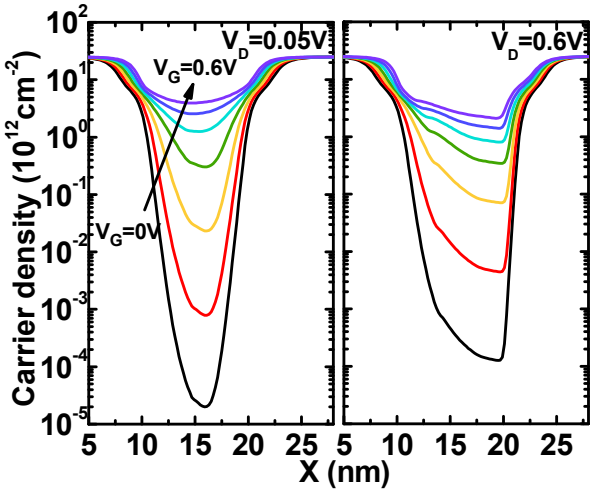


Fig. 4. Carrier densities along the transport direction in linear and saturation state with various gate voltages.

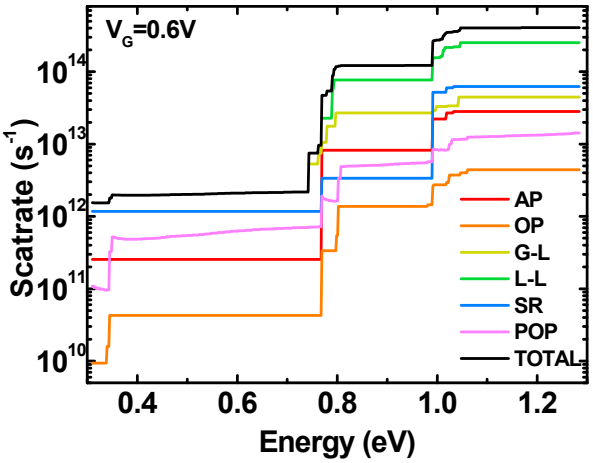


Fig. 5. Electron scatter rate spectrum. AP: intra valley acoustic phonon scattering, OP: intra valley optical phonon scattering, Γ-L: inter valley optical phonon scattering between Γ and L valleys, L-L: inter valley optical phonon scattering among L valleys, SR: surface roughness scattering, POP: polar optical phonon scattering. TOTAL: total scattering rate.

The subbands along the transport direction with gate bias of 0.6V and drain voltage of 0.6V are plotted in Fig. 3. The energy gap between the Γ and L valleys is 0.49eV which is much smaller than the bulk material (0.67eV) because the subband energy in Γ valley is lifted in a bigger magnitude by the quantum confinement effect due to its extremely small effective mass along the confinement direction. The electron density distribution along the channel at drain biases of 0.05V and 0.6V under different gate biases are depicted in Fig.4.

The scattering rate versus energy is plotted in Fig. 5. The lowest energy is not 0 eV but 0.31 eV due to the effect of the quantum confinement. The scattering rate is about $10^{12}$ s$^{-1}$ in low energy region. This is much lower than that of Si (above $10^{13}$ s$^{-1}$), which corresponds to the high mobility property of III-V material. However, when the kinetic energy is higher than 0.8 eV, the inter-valley scattering mechanisms show up and the scattering rate increases dramatically to $10^{14}$ s$^{-1}$ because of the increasing density of state brought about by the population of the higher L valleys. To investigate the effect of higher scattering rate, the scattering probabilities of every

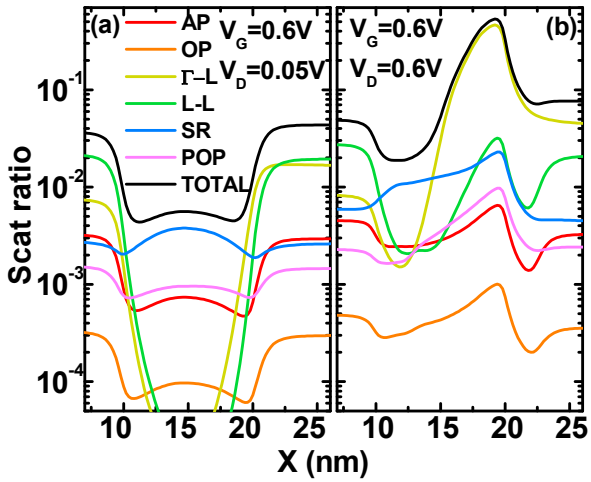


Fig. 6. The ratio of electrons scattered by different scattering mechanisms along the channel, (a) $V_D$=0.05V and (b) $V_D$=0.6V. The surface roughness scattering takes the dominate place in low $V_D$ case, while the inter-valley scattering plays a more important role when $V_D$ is higher.

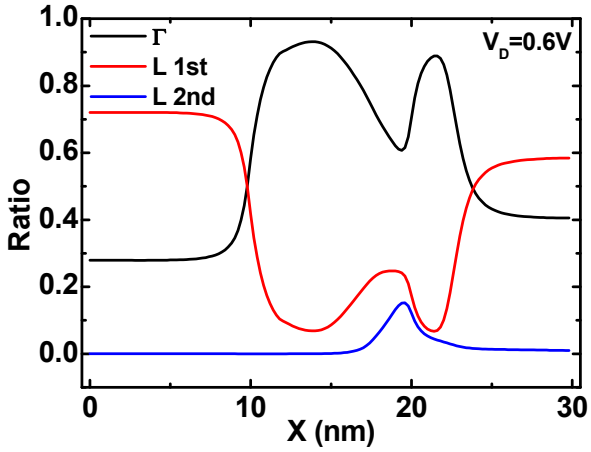


Fig. 7. The subband occupancy rate in Γ and L valleys along the transport direction with $V_D$=0.6V. The effect of inter-valley scattering is very obvious near the end of the channel.

scattering mechanism along the channel under the drain bias of 0.05V and 0.6V are compared and plotted in Fig. 6. In low $V_D$ case depicted in Fig. 6(a), the total scattering probability along the channel is lower than 1%. The most predominant scattering mechanism is surface roughness scattering while the effect of the inter-valley scattering can be ignored. When the drain bias is increased to 0.6 V, as shown in Fig. 6(b), the SR scattering mechanism still plays an important role, especially at the beginning of the channel. However, during the acceleration process, the rates of inter-valley scattering increase significantly and become the highest at the end of the channel. Fig. 7 shows the occupancy rate of different subbands along the channel with $V_G$=0.6V and $V_D$=0.6V. It can be seen that the carriers are mostly populated in L valleys whose energy is relatively higher in the source and drain due to the large carrier density and the tiny density of state in the Γ valley. Carriers are pushed up to the L valleys according to the Pauli's exclusion principle. In the channel, the occupancy rate of the Γ valley increases rapidly due to the much smaller carrier density. When the carriers get enough energy during the transport process, the inter-valley scattering begins to show up. It can be seen that

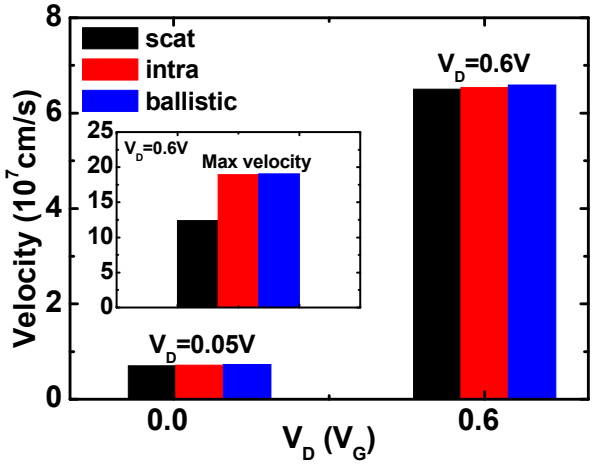


Fig. 8. The inject velocity of electrons under several of drain voltage with different scattering conditions. The inset figure shows the maximum average velocity in the channel when $V_D$=0.6V. The injection velocity is hardly affected by the scattering mechanisms while the maximum velocity is relatively more sensitive.

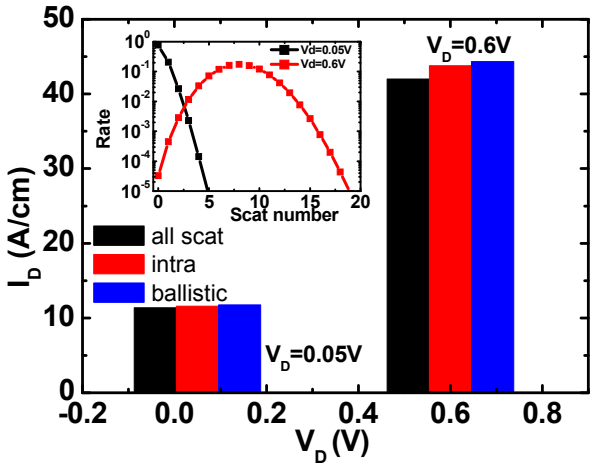


Fig. 9. The effect of different scattering mechanisms on the drain current with various $V_D$. The gate voltage is 0.6V. The inset figure shows the probability distribution of the number of scattering that the electrons encounter in the channel.

more than 1/3 of the carriers are scattered to the L valleys from the Γ valley. This corresponds to the higher scattering rate under stronger drain bias shown in Fig. 6.

To evaluate the effect of the scattering on the drive current, according to the top-of-the-barrier model [17, 18], the injection velocity at the virtual source and the maximum velocity in the channel under different scattering mechanisms are extracted in Fig. 8. The intra-valley scattering has little effect on both the injection velocity and the maximum velocity because of their low scattering rates. However, when the inter-valley scatterings are considered, the maximum velocity in the high $V_D$ bias case is dropped by more than 1/4 because the transport effective mass of the L valleys is much higher than that of Γ valley. Fig. 9 shows the contrast among the current under different scattering mechanisms. The inset is a probability distribution of the scattering number that the electrons encounter during transport. When the drain bias is 0.05 V, the electrons can almost transport through the channel in an absolute ballistic way, but approximately 8-10 times of scattering are

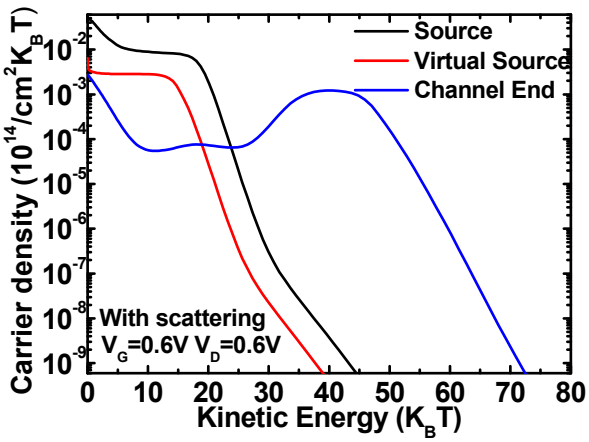


Fig. 10. The kinetic energy distribution at source, virtual source, the channel end with $V_G$=0.6V and $V_D$=0.6V. The distribution function in the channel end deviating from the thermal equilibrium state indicates the quasi-ballistic transport mechanism in the device.

encountered in the high $V_D$ case. As a result, the effect of scattering on the drive current becomes obvious under a high longitudinal electric field. The ballistic ratio B ($I_{scat}/I_{ball}$) decreases from 96.8% to 94.5%. Nonetheless, the features of the quasi-ballistic transport still exist as shown in the energy distribution plotted in Fig. 10. At the source and the VS, the electrons distribute in equilibrium state. However, the shape of the distribution function is different in the drain as the fraction of the electrons populated in higher energy states increases significantly.

## IV. Conclusion

The scattering details of an ultra-short $In_{0.53}Ga_{0.47}As$ double gate nMOSFETs are investigated by a deterministic BTE solver. The results show that the scattering has little effect on the current at a low $V_D$ bias but to some extent impedes the transport of the electrons under a high $V_D$. The dominant scattering mechanisms are surface roughness and the inter-valley scatterings. The ballistic ratio decreases from 96.8% to 94.5% when the drain bias increases from 0.05V to 0.6V.

## Acknowledgment

This work was supported by the National Natural Science Foundation of China under Grant 61404005 and 61421005.

## References

[1] S. Takagi, M. Takenaka, “Ge/III-V MOS device technologies for low power integrated systems”, Solid State Device Research Conference ESSDERC, 2015.

[2] J. A. Del Alamo, “Nanometre-scale electronics with III-V compound semiconductors”, Nature, vol. 479, pp. 317-323, 2011.

[3] K. Kalna, L. Yang, and A. Asenov, “Monte Carlo simulations of sub-100 nm InGaAs MOSFETs for digital applications”, Solid-State Device Research Conference, ESSDERC, pp.169-172, 2005.

[4] P. Palestri, D. Esseni, S. Eminente, C. Fiegna, E. Sangiorgi, and L. Selmi, “Understanding quasi-ballistic transport in nano-MOSFETs: part I-scattering in the channel and in the drain”, Electron Devices, IEEE Transactions on, vol. 52, pp. 2727-2735, 2005.

[5] A. Svizhenko, M. P. Anantram, “Role of scattering in nanotransistors.”, Electron Devices, IEEE Transactions on, vol. 50, pp. 1459-1466, 2003.

[6] G. Liu, G. Du, T. Lu, X. Liu, P. Zhang, and X. Zhang, “Simulation study of quasi-ballistic transport in asymmetric DG-MOSFET by directly solving Boltzmann transport equation.”, Nanotechnology, IEEE Transactions on, vol. 12, pp. 168-173, 2013.

[7] T. Lu, G. Du, X. Liu, and P. Zhang, “A finite volume method for the multi subband Boltzmann equation with realistic 2D scattering in double gate MOSFETs.”, Communications in Computational Physics, vol. 10, pp. 305-338, 2011.

[8] S. Di, K. Zhao, T. Lu, G. Du, and X. Liu, “Investigation of transient responses of nanoscaletransistors by deterministic solution of the time-dependent BTE.” Journal of Computational Electronics, 2016.

[9] S. Di, K. Zhao, Z. Lun, T. Lu, G. Du, and X. Liu, “Simulation of nano-scale double gate $In_{0.53}Ga_{0.47}As$ nMOSFETs by a deterministic BTE solver.”, International Symposium on VLSI Technology, Systems and Application (VLSI-TSA), IEEE, April, 2016.

[10] F. Filbet, and G. Russo, “High order numerical methods for the space non-homogeneous Boltzmann equation”, Journal of Computational Physics, vol. 186, pp. 457-480, 2003.

[11] N. B. Abdallah, M.J. C’aceres, J.A. Carrillo, et al. “A deterministic solver for a hybrid quantum-classical transport model in nano MOSFETs”, Journal of Computational Physics, vol. 228, pp. 6553–6571, 2009.

[12] S. Smirnov, “Physical Modeling of Electron Transport in Strained Silicon and Silicon- Germanium.”, PhD thesis, Fakultät für Elektrotechnik und Informationstechnik, von, Wien, Österreich, 2003.

[13] D. Esseni, P. Palestri, and L. Selmi, “Nanoscale MOS Transistors: Semi-Classical Transport and Applications.”, Cambridge university press, 2011.

[14] D. Esseni, “On the modeling of surface roughness limited mobility in SOI MOSFETs and its correlation to the transistor effective field.” Electron Devices, IEEE Transactions on, vol. 51, pp. 394-401, 2004.

[15] M. V. Fischetti, “Monte Carlo simulation of transport in technologically significant semiconductors of the diamond and zinc-blende structures. I. Homogeneous transport.”, Electron Devices, IEEE Transactions on, vol. 38, pp. 634-649, 1991.

[16] http://www.itrs.net/.

[17] M. Lundstrom, “Elementary scattering theory of the Si MOSFET.”, Electron Device Letters, IEEE, vol. 18 pp. 361-363, 1997.

[18] M. Luncstrom and Z. Ren, “Essential physics of carrier transport in nanoscale MOSFETs”, Electron Devices, IEEE Transactions on, vol. 49, pp. 133-141, 2002.